Effects of the extensional rheological properties of polymer solutions on vortex shedding and turbulence characteristics in a two-dimensional turbulent flow

Hidema, Ruri
Murao, Ikumi
Komoda, Yoshiyuki
Suzuki, Hiroshi

(Citation)
Journal of Non-Newtonian Fluid Mechanics,254:1-11

(Issue Date)
2018-04

(Resource Type)
journal article

(Version)
Accepted Manuscript

(URL)
https://hdl.handle.net/20.500.14094/90004878

Effects of the extensional rheological properties of polymer solutions on vortex shedding and turbulence characteristics in a two-dimensional turbulent flow

Ruri Hidema*, Ikumi Murao, Yoshiyuki Komoda, Hiroshi Suzuki

Department of Chemical Science and Engineering, Kobe University, Kobe 657-8501, Japan

*Corresponding Author
Phone: +81-78-803-6657
Fax: +81-78-803-6657
hidema@port.kobe-u.ac.jp

An experimental study was performed to investigate the relationship between the extensional rheological properties of polymer solutions and vortex deformation in turbulent flow. Polyethyleneoxide as a flexible polymer and hydroxypropyl cellulose as a rigid polymer are added to two-dimensional (2D) turbulent flow. Specifically, 2D flow is advantageous as it examines the effect of the extensional rheological properties of polymers on the flow. In the study, 2D turbulent flow and vortex shedding in 2D turbulent flow were observed using interference patterns and particle image velocimetry (PIV). Power spectrum of the 2D flow images and 2D turbulence statistics calculated by PIV analysis indicated that there are three flow regimes of vortex shedding in the 2D turbulent flow of the polymer solution. The vortex shedding in the 2D flow was categorized into three types, and this was affected by the relaxation time of the polymer solutions.

Keywords: Extensional rheological properties, Relaxation time, Two-dimensional turbulent flow, Vortex shedding, Polymer solution, Drag reduction

1. Introduction

Research attention has focused on polymer drag reduction for more than half a century. During the period, a large number of experimental studies were conducted [1-9]. Turbulence statistics of a flexible polymer solution and a rigid polymer solution were compared, and subsequently type A and B drag reduction, and low and high drag reduction were suggested [10-16]. The most important feature of drag reduction is that the polymer additives do not simply suppress turbulent motion: the turbulent fluctuation in the streamwise direction increases while the normal turbulent intensity decreases. The effect is anisotropic [6-8, 17-23]. Vortices that are generated at the wall in a flow undergo deformation when drag reduction occurs [7, 8, 21-23]. The anisotropy of turbulence is due to the

deformation of vortices. Motozawa et al. [8] proposed a model for vortex variation near a wall with polymer additives. However, the background mechanism of drag reduction is not completely clarified to date.

The complexity of the phenomenon stems from interactions between vortices and polymers in the turbulent flow. Polymer molecules are larger than solvent molecules although the polymer molecules are significantly smaller than the smallest vortex sizes in the flow. It is considered that stretched polymers play a role in the phenomena. The main questions on the phenomenon are related to the manner in which the polymers interact with vortices, namely polymer characteristics that affect turbulence.

Many numerical studies were performed to clarify the anisotropic effect of polymers on drag reduction. Toonder et al. [4] proposed an extensional viscosity model — viscous anisotropic effects of extended polymers — that is essential for turbulent drag reduction. However, the extensional viscosity model is unable to predict the onset of drag reduction. Therefore, Min et al. [17] adopted the elastic theory wherein the study derived transport equations for kinetic energy and elastic energy. Kinetic energy is transported through the elastic energy of polymers in a turbulent flow. To achieve energy transportation, a time criterion is important. Min et al. [17] suggested that the relaxation time of a polymer should be sufficiently long to transport elastic energy from the near-wall region to the buffer or log layer. In the study, the time criterion was defined based on wall shear velocity.

Both experimental [6-8] and numerical [17-23] studies captured vortex deformations. However, the index or criteria proposed in these studies was derived based on shear stress: the time criterion or rheological properties were defined by physical properties based on shear stress. While these studies discussed extensional viscosity or extensional rheological properties, it is not possible to separate the effects of extensional stress on polymers from the effects of shear stress. Therefore, the effects of extensional rheological properties of polymers will be clearer if we observe a turbulent flow that is mainly affected by extensional stresses.

To focus on extensional rheological properties of a polymer solution in a flow, we used a flowing soap film, namely a quasi-two-dimensional (2D) flow, to realize a turbulent flow that was mainly affected by extensional stresses [24-26]. The flowing soap film is surrounded by air, and therefore the 2D flow is free from shear stresses that are due to the existence of solid walls. Additionally, an

extensional flow occurs at the comb when a comb that consists of equally spaced cylinders is inserted into the 2D flow. The comb generates vortices that merge into others. The 2D turbulent flow is the result of merger of several vortices in which vortices that are generated in the flow characterize the turbulence. Thus, for the case in which polymers are added to the flow, polymers affect the 2D turbulence. Therefore, we focus on the effects of the extensional properties of polymer solutions on the 2D turbulence where it is possible to almost neglect the effects of shear stress.

Variation in the 2D turbulence that was caused by polymers was reported in previous studies [27, 28]. Flowing soap films were used as a test field of the 2D turbulence. The studies reported that the polymers suppress large scale fluctuation of thickness fluctuation in the flowing soap films, and this is because energy transfer is prevented due to the polymers [28]. In our previous studies [29-31], we compared the effects of a flexible and a rigid polymer on 2D flow. Vortices in 2D turbulent flow exhibited deformation with polymers. It is suggested that the prohibition of energy transfer in the flow varied due to the rigidity of polymers [31].

The vortices in 2D turbulent flow were generated at the comb in the flow, and thus the present study involved an experimental investigation that focuses on vortex shedding characteristics at cylinders in 2D flow. The 2D turbulent flow system allows us to consider vortex characteristics affected by extensional rheological properties under extensional stress. In a previous study, Cressman et al. [32] studied the effect of polymers on vortex shedding in a 2D flow. The vortex was deformed with polymer additives. Cressman et al. discussed the effect of the extensional viscosity of polymer solution on the vortex deformation although they did not quantify extensional rheological properties. We conducted a more precise study on the vortex deformation, and we also mention the connection between the deformation of vortices and turbulent drag reduction.

Specifically, 2D turbulent flow and vortex shedding are visualized using interference patterns of the film. The velocity fields close to the cylinders are captured by particle image velocimetry (PIV), and the flow statistics are discussed. The extensional rheological properties of flexible and rigid polymer solutions are measured, and the effect of extensional rheological property on vortex shedding is clarified in terms of relaxation time and vortex shedding time.

2. Experimental Procedures

2.1. Materials

Sodium dodecylbenzenesulfonate (SDBS) was dissolved in pure water at a concentration of 2 wt%. Polyethyleneoxide (PEO, molecular weight: 3.5×10^6) was used as a flexible polymer wherein concentrations were varied as 0.25, 0.5, 0.75, 1.0, 1.25 and 1.5×10^{-3} wt%. As rigid polymers, hydroxypropylcellulose (HPC, molecular weight: $>1.0\times10^6$) was used at concentrations of 0.01, 0.02, and 0.05 wt%. The overlap concentration of PEO is approximately 1.2×10^{-2} wt%, and that of HPC is approximately 0.15 wt%.

2.2. Viscosity and relaxation time measurements

The viscosity of the sample solutions was measured by using a rheometer (MCR301: Anton Paar) with a cone-plate device at shear rates from 1 to 1000 s^{-1}. The relaxation time of the sample solutions under extensional stress was measured by a capillary break up extensional rheometer (CaBER, Thermo scientific). The diameter of the end plate of CaBER was 6 mm, the initial distance between two end plates was set as 3 mm, and the final distance between two plates was adjusted as 8 mm. The diameter of the neck of the fluid, D [mm], was plotted relative to time, t [s]. The diameter was fitted using the fitting function, $D=A\exp(-t/3\lambda)$ to calculate each relaxation time under extensional stress, λ [s], of each sample solution. Here, A [m] is a constant that was determined by the experiment. The extensional property of sample solutions was evaluated by the relaxation time in this study because the absolute value of the dilute solution extensional viscosity is not completely reliable.

2.3. Experimental apparatus used to create flowing soap films

The experiments were performed using the apparatus shown in Fig.1. The complete image of the apparatus is shown in Fig.1(a). The outline of our apparatus follows that in previous studies [29-31] as originally proposed by Rutgers et al [33]. The channel was composed of two nylon wires tightened by a weight. Gravity-driven sample solutions flew between the two wires to create flowing soap films. The flow rate, Q [L/s], was controlled by a valve connected to an injection nozzle. The flow rate was measured by a flow meter (KEYENCE, FD-SF1). First, it was maintained constant at 25 ml/min. While the flow is gravity-driven, the velocity

reaches a constant value at approximately 300 mm behind the injection nozzle [33]. The mean velocity, V [m/s], was 1.37 m/s when the flow rate was 25 ml/min. The Reynolds number as calculated by the mean velocity, water viscosity, diameter of the cylinder (3 mm), and water density was approximately 4,600. The mean thickness of the water layer, h [m], was approximately 3 μm, and this was derived from the relationship between h, V, and Q, and the width of the channel W [m], that is, $h = Q / (V \cdot W)$.

To create 2D turbulence on the flowing soap films, the comb composed of seven equally spaced cylinders was inserted perpendicular to the flow at 130 mm downstream from the beginning of the parallel section in the channel. Figure.1(b) is a close-up of the figure showing the comb and the flow around it. The diameter of the cylinder was 3 mm, and the gap between cylinders was 9 mm. The flow passing through between the cylinders was affected by extensional rates, $\dot{\varepsilon} = 260$ s^{-1} in which $\dot{\varepsilon}$ was calculated by the following equation [29-31]:

$$S(t) = S_0 \exp(-\dot{\varepsilon} t) \quad (1)$$

Specifically, S_0 [m^2] is the cross-sectional area of the water layer before deformation, $S(t)$ [m^2] is the cross-sectional area after deformation, and t [s] is the time required for deformation from S_0 to $S(t)$. Here, S_0 was calculated as 72 mm × 3.0 μm, $S(t)$ was calculated as 54 mm × 3.0 μm, and t was calculated by the radius of the cylinders and the mean velocity of the flow (i.e., 1.5 mm divided by 1.37 m/s). Here, $\dot{\varepsilon}$ was calculated as 260 s^{-1}. Thus, it is possible to stretch and orient polymers in the flow due to $\dot{\varepsilon}$=260 s^{-1}, and this affects vortex shedding at the comb on the 2D flow.

Given that $\dot{\varepsilon}$ affects rheological properties of the polymer solution, it is necessary to observe the effects of $\dot{\varepsilon}$. Thus, $\dot{\varepsilon}$ was varied by controlling the flow rates. Here, we changed the flow rates of the PEO solution from 25 ml/min to 45 ml/min, and this indicates that $\dot{\varepsilon}$ approximately corresponds to the range of 260–355 s^{-1}.

We observed the flow at two positions by using two methods. The first observed area is termed test section 1 and was from immediately under the comb to 100 mm downstream with a 45-mm span-wise width. The second observed area is termed test section 2, and it was 150 mm downstream from the comb to 200 mm

downstream with a span-wise width of 45 mm (Fig.1c). The precise method to observe the flow is described in the following sections.

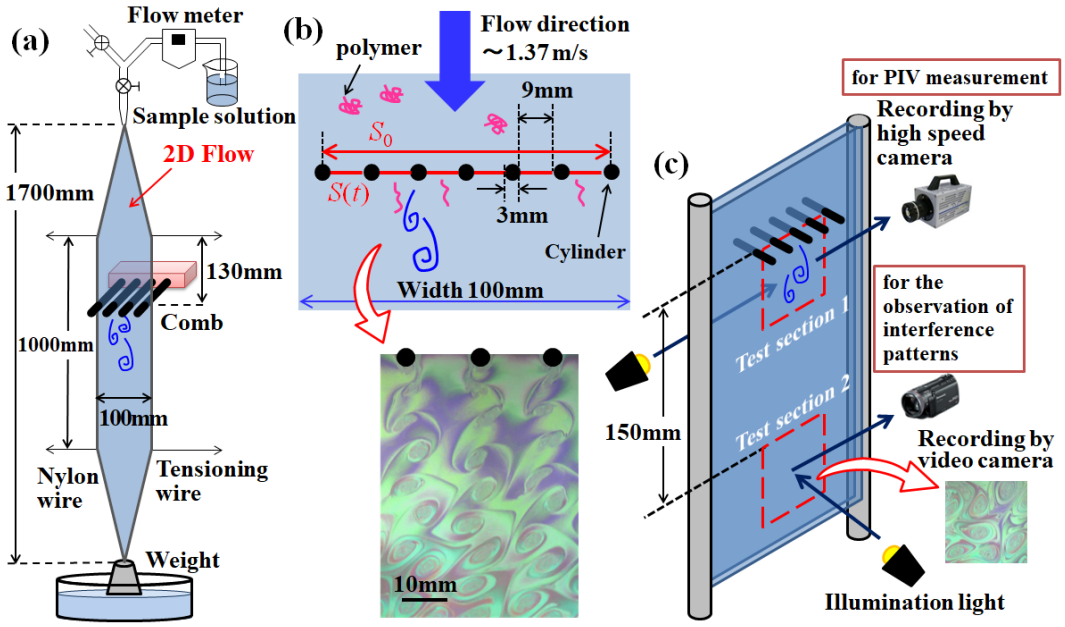

Fig.1 Schematic of the experimental apparatus

2.4. Visualization of the flow by interference patterns and single image analysis

In 2D flows, vortices shed at the comb were advected downstream without significant deformation. Vortex shedding at the comb and the advected vortices in the 2D flow were visualized at test sections 1 and 2 through interference patterns of the film. Commercial white lights (Toshiba, EFA25EN/22) illuminated the flow, and the illumination lights were reflected on the front and back surfaces of the film. The reflected lights interfered with each other, and this led to interference patterns. The interference patterns include information on the thickness of the water layer in the film, i.e., 2D flow. Therefore, we use the interference pattern to observe and analyze the 2D flow. The interference images of the flowing soap films were recorded by using a digital video camera (Panasonic TM700) in the test sections. The shutter speed of the video camera was set at 1/3,000 s. The time interval for a series of images was adjusted to 1/60 s. Each of the frames recorded by the camera was converted into an RGB file with a spatial resolution of 640 × 360 pixels, and this corresponds to 42 × 23 mm^2.

Part of the image, 256 × 256 pixels, was clipped from a still image recorded at test section 2. The clipped image was analyzed by 2D-FFT to obtain a power spectrum, $<I^2(k_x, k_y)>$, of the image. The power spectrum, $<I^2(k_x, k_y)>$, was calculated based on the pixel intensity of G with a Hamming window where k_x m^{-1} and k_y m^{-1} denote the spatial wavenumber in the streamwise and normal directions in the interference image, respectively. The pixel intensity of G was selected to avoid variation in an order of interference in the data acquisition area [34, 35]. The power spectrum exhibits scaling behaviour as $<I^2(k_x, k_y)> \sim k_x^{\alpha}$ and $<I^2(k_x, k_y)> \sim k_y^{\beta}$ in the streamwise and normal directions, respectively. As described above, the interference patterns reflect the thickness of the water layer. Additionally, the fluctuation in the thickness is a passive scalar in the 2D flow [36, 37]. Therefore, the scaling index of the power spectrum follows passive scalar scaling in 2D flow. The scaling index is informative to evaluate energy transfer in 2D flow [31].

2.5. Measurement and analysis of velocity fields by using PIV

Particle Image Velocimetry (PIV) was used to obtain velocity fields in the test section 1. Local flow fluctuates around the grids and gradually approaches steady flow with increases in the distance from the comb. Therefore, only the test section 1 was measured by PIV. Polystyrene particles with a diameter of 2.11 μm were seeded at a concentration of 1.12×10^{-2} vol% as tracer particles for PIV measurements. To visualize the tracer particle trajectories around the grid, bright light sources and a high-speed video camera were prepared. A mercury lamp (Photron, HVC-SL) and two halogen lamps (Takagi, WLT-30) were set behind the flowing soap films. A high-speed video camera (Photoron, FASTCAM SA3) was set in front of the soap film as shown in Fig.1(c). The shutter speed of the video camera was 1/10,000 s, and the time interval between two frames was adjusted to 1/3,200 s.

A commercial software (LaVision 8) was used to calculate velocity fields from a series of images (See Fig.8). Fluctuation intensities and the vorticity of the flow fields were calculated by using local velocity. Fluctuation intensities, FI_{V_x} and FI_{V_y}, were calculated in the streamwise and normal directions, respectively, as described in corresponding Eqs.2 and 3. In order to obtain a smooth line of the fluctuation intensity as shown from Fig. 10 to Fig. 14, 3200 instantaneous velocity

fields were used to calculate average values of FI_{V_x} and FI_{V_y}. The frame rates of the high-speed camera to obtain the velocity fields was 3200 fps.

$$FI_{V_x} = \frac{\sqrt{\left(\overline{V}_x - V_x\right)^2}}{\overline{V}_x} \quad (2)$$

$$FI_{V_y} = \frac{\sqrt{\left(\overline{V}_y - V_y\right)^2}}{\overline{V}_x} \quad (3)$$

Here, $\overline{V}_x$ [m/s] and $\overline{V}_y$ [m/s] are the mean velocities in the streamwise and normal directions, respectively, and V_x [m/s] and V_y [m/s] are the local instantaneous velocities in the streamwise and normal directions, respectively. The fluctuation intensities shown in Fig.10 to Fig.14 were normalized with mean velocity, $\overline{V}_x$. The Reynolds stress, $-\overline{v_x v_y}$, was also calculated using Eq.(4), and this is shown in Fig.15 and Fig.16. The expression is as follows:

$$-\overline{v_x v_y} = -\left(\overline{V}_x - V_x\right)\left(\overline{V}_y - V_y\right) \quad (4)$$

The vorticity, $\omega(x, y)$ [s^{-1}], is described as follows:

$$\omega(x,y) = \left(\frac{\Delta V_y}{\Delta x} - \frac{\Delta V_x}{\Delta y}\right) \quad (5)$$

Local velocity gradients, $\Delta V_y / \Delta x$ [s^{-1}] and $\Delta V_x / \Delta y$ [s^{-1}] were calculated using four neighbour cells, (i, j), $(i+1, j)$, $(i, j+1)$, and $(i+1, j+1)$ as follows:

$$\frac{\Delta V_y}{\Delta x} = \frac{\dfrac{V_y(i,j+1) - V_y(i,j)}{\Delta x} + \dfrac{V_y(i+1,j+1) - V_y(i+1,j)}{\Delta x}}{2} \quad (5)$$

$$\frac{\Delta V_x}{\Delta y} = \frac{\dfrac{V_x(i+1,j) - V_y(i,j)}{\Delta y} + \dfrac{V_x(i+1,j+1) - V_x(i,j+1)}{\Delta y}}{2} \quad (6)$$

Here, Δx[m] and Δy[m] are the distances of the velocity grids for the streamwise and normal directions, respectively.

3. Results and Discussion

3.1. Rheological properties of the sample solution.

Zero shear viscosities, η_0 [mPa·s], and relaxation times, λ [ms], of the

sample solutions are given in Table 1. Specifically, η_0 of the sample solutions that contain PEO was almost identical to that of the polymer-free solution; and η_0 of the sample solutions that contain HPC was slightly higher. Additionally, λ of the polymer-free solution was really low; and λ of the PEO solutions exceeded that of the polymer-free solution and the HPC solutions. The relaxation time is related to the extensional viscosity of the solution. Therefore, the extensional viscosity of the PEO solution is expected to exceed that of the HPC solution.

Table 1. Rheological properties of the sample solutions

		Zero shear viscosity η_0 [mPa·s]	Relaxation time λ [ms]
Polymer free solution		1.08	0.345
PEO Concentration [$\times 10^{-3}$wt%]	0.25	1.09	4.16
	0.50	1.10	7.01
	0.75	1.13	9.78
	1.0	1.12	12.8
	1.25	1.12	15.8
	1.5	1.16	18.9
HPC Concentration [wt%]	0.01	1.21	4.43
	0.03	1.72	4.25
	0.05	2.52	4.53
	0.08	3.11	4.40

3.2. Laminarization of 2D turbulence with polymer additives

Figure 2 shows the 2D flow at the test section 2 as visualized by the interference patterns. In the case of the polymer-free solution, vortices in 2D turbulent flow grew larger in the downstream region as shown in Fig. 2(a). On the other hand, vortices in the flow grew long and thin when PEO was added at 1.5×10^{-3} wt% (Fig. 2(b)). However, in the case of the HPC solution, vortices almost identical to those in the case of the polymer-free solution were observed in Fig. 2(c). To quantify these images, we calculated the power spectrum, $\langle I^2(k_x, k_y)\rangle$, of these images in both the streamwise and normal directions. The power spectrum exhibits scaling behaviour in both directions as $\langle I^2(k_x)\rangle \sim k_x^{\alpha}$ and $\langle I^2(k_y)\rangle \sim k_y^{\beta}$. Here α and β denote the scaling indices in streamwise and normal directions, respectively. An example of the power spectrum fitted by a power function was reported in our previous study [31]. As shown in Fig. 3, the scaling indices of the

polymer-free solution, namely α and β, were -5/3. This value appears when the flow is dominated by inverse energy cascade that is a feature of 2D turbulence [29-31, 37]. The scaling indices, α and β, approached a value of -1 asymptotically when PEO was added to the flow. Specifically, the scaling index in the case at the concentration of 0.75×10^{-3} wt% exhibited a sudden increase. This result indicated that the flow significantly changed at this concentration. In our previous study, we also measured friction coefficients of the PEO solution in a pipe. The results indicated that the drag reduction appeared at concentrations exceeding that of the 0.75×10^{-3} wt% PEO solution [29]. Conversely, in the case of the HPC solution, the variations in the indices with the concentration were lower than those of the PEO solution with respect to the overall concentration. The variation in the scaling index is due to the prohibition of energy transfer in the 2D turbulent flow [28]. Our previous studies [29-31] suggested that the extensional viscosity and the orientation of polymers in the flow prohibited energy transfer. The relaxation time related to extensional viscosity of the PEO solution exceeded that of the HPC solution. Therefore, the variation in the scaling index of the PEO solution exceeded that of the HPC solution.

The extensional rheological property of the PEO solutions was significantly affected by the concentrations and extensional rate that was added to the solution, and thus the effects of the extensional rate on the flow of the PEO solution were examined. Figure 4 shows the scaling index of the power spectrum of the PEO solution at each extensional rate. In the streamwise direction, the scaling index α of the polymer-free solution and 0.5×10^{-3} wt% PEO solution was almost constant at all the extensional rates. Conversely, the scaling index α of the 1.0×10^{-3} wt% PEO solution increased with the extensional rate. In the normal direction, the scaling index β of all the solutions was almost constant at all the extensional rates. We consider that the tendency of the scaling index in streamwise and normal directions also confirms the mechanism of energy transfer in 2D turbulent flow as suggested in our previous studies. The extensional viscosity prohibits energy transfer in the streamwise direction, and the orientation of polymers in the flow prohibits energy transfer in the normal direction.

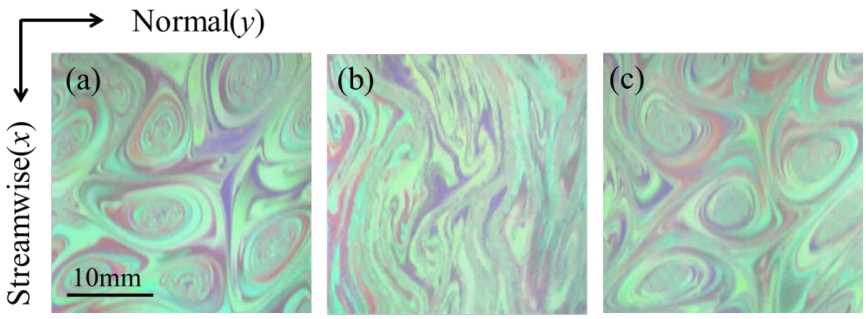

Fig.2 Interference images of 2D turbulent flow in test section 2. The sample solutions are (a) Polymer-free solution, (b) PEO1.5×10^{-3} wt% solution, and (c) HPC 0.08 wt% solution.

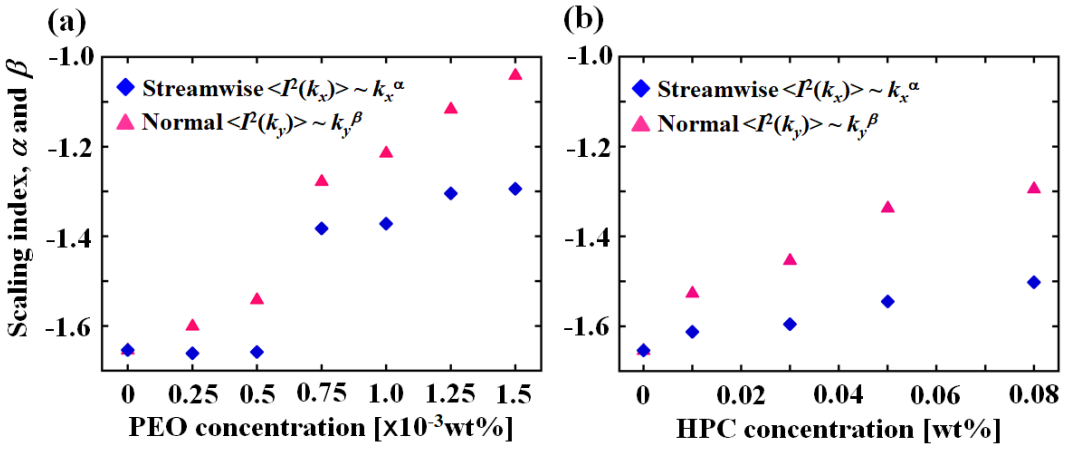

Fig.3 Scaling index of the power spectrum in the streamwise and normal directions. (a) PEO solution and (b) HPC solution.

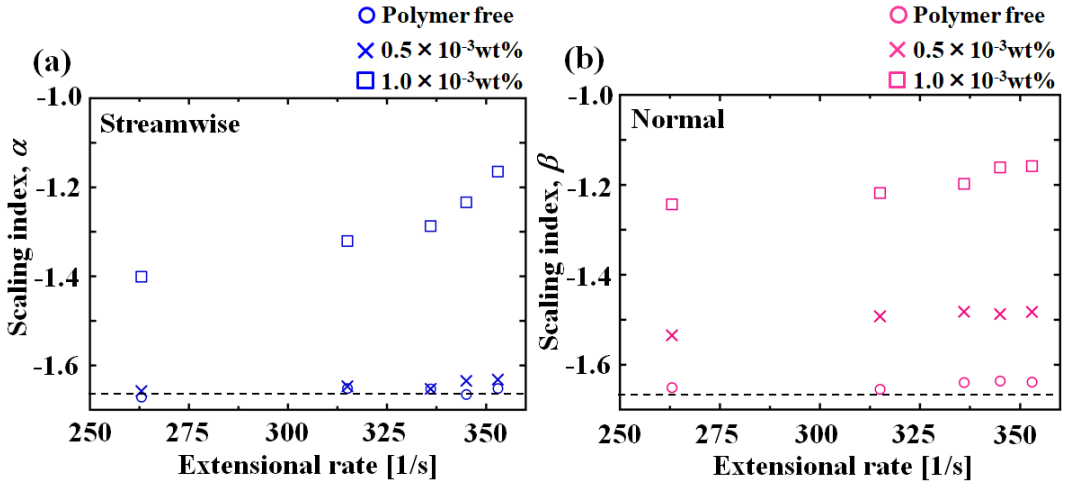

Fig.4 Extensional rate dependence of the scaling index calculated by the power spectrum of the polymer-free, PEO 0.5×10^{-3} wt%, and PEO 1.0×10^{-3} wt% solution. (a) Streamwise direction, (b) Normal direction. The dot-line denotes the value of -5/3.

3.3. Vortex shedding at the comb affected by polymers

Vortices on 2D turbulent flow observed at test section 2 were shed at the comb and were advected to the downstream. Thus, the vortex shedding at the comb is potentially affected by polymers when the vortices at test section 2 were deformed. Therefore, the vortex shedding at the comb was visualized through interference patterns, and velocity fields were measured by PIV. Figures 5 and 6 show the vortex shedding from a cylinder of the comb in each solution. These images were obtained at test section 1. The black circles represent the cylinders of the comb. In the case of the polymer-free solution, the vortex exhibited shedding immediately after the cylinder (Fig.5(a)). The vortex gradually increased with increases in the distance from the cylinder and merged with other vortices downstream. The wake region behind the cylinder was expanded when the PEO concentrations increased to 0.25 and 0.5×10^{-3} wt%, (Fig.5(b), (c)). Thus, the position where vortices were generated shifted downstream. Here, we define the vortices observed at a concentration lower than 0.5×10^{-3} wt% as Vortex-Type1. Subsequently, in the case of the PEO 0.75×10^{-3} wt% solution, vortices almost disappeared in test section 1 (Fig.5(d)). Here, we define the diminished vortex as Vortex-Type2. Vortices appeared again under the cylinder when the concentration of PEO exceeded 1.25×10^{-3} wt%, which is defined as Vortex-Type3. However, Vortex-Type3 was observed in 1.25 and 1.5×10^{-3} wt% of the PEO concentrations and was significantly different from the original vortex, namely Vortex-Type1. In previous numerical simulation studies, vortices similar to the three types of vortices observed in the present study were suggested [38].

Figure 6 shows the interference patterns of the 2D flow of the HPC solution in test section 1. In the case of the HPC solution, Vortex-Type1 was observed at all the concentrations. The wake region behind the cylinder was expanded to the downstream with increases in the concentration of HPC. However, the vortices did not disappear. Vortex-Type2 and Vortex-Type3 were not observed in the flow of the HPC solution.

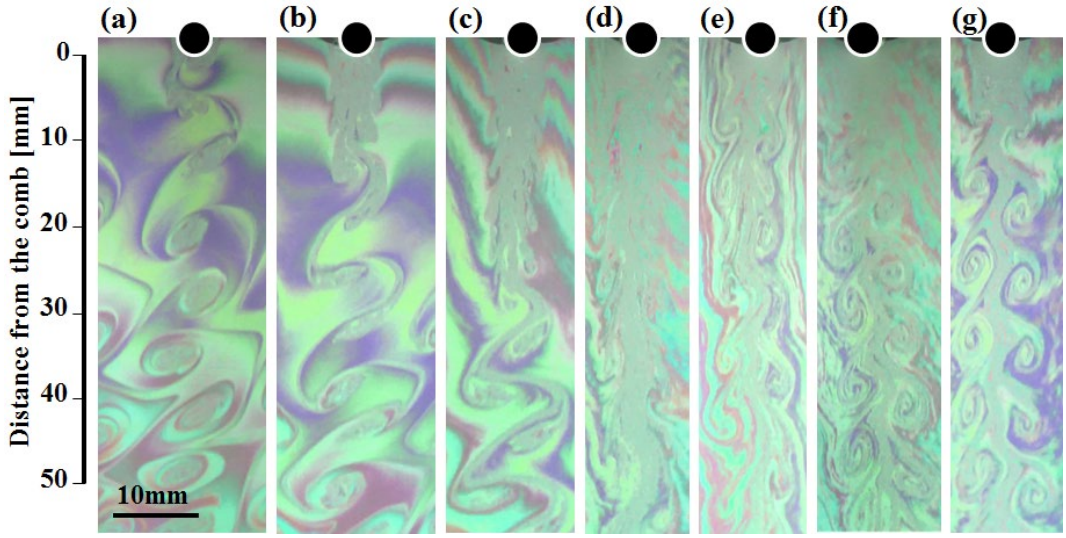

Fig.5 Interference patterns of vortex shedding in the PEO solution obtained at the test section 1. In the figure, we focus on a cylinder of the comb. (a) is the flow of the polymer-free solution. Figures 5(b), 5(b), 5(c), 5(d), 5(e), 5(f), and 5(g) denote the flow of the PEO solution at the concentrations of (b) 0.25, (c) 0.5, (d) 0.75, (e) 1.0, (f) 1.25, and (g) 1.5×10^{-3} wt%, respectively.

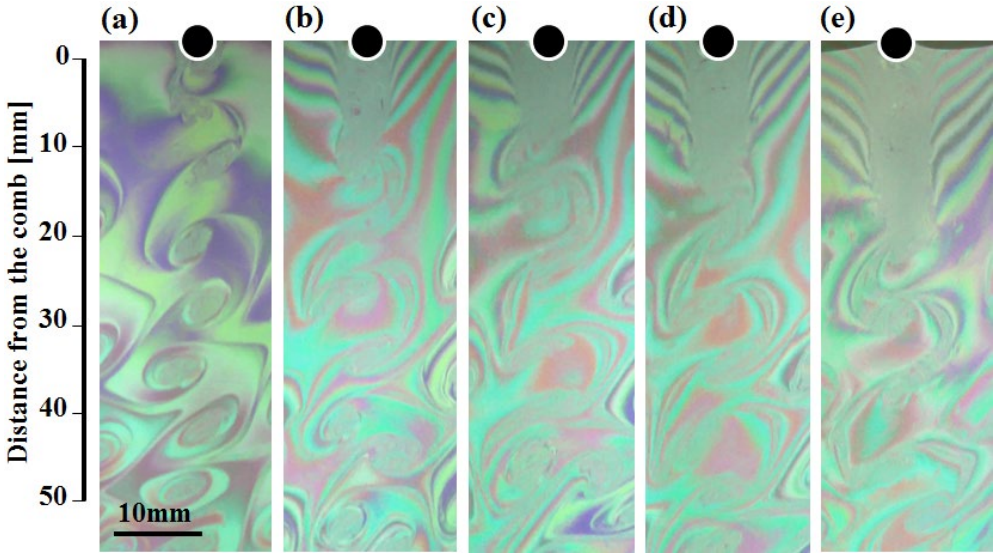

Fig.6 Interference patterns of vortex shedding in the HPC solution obtained at the test section 1. (a) is the flow of the polymer-free solution. From (b) to (e) are the flows of the HPC solution at the concentration of (b) 0.01, (c) 0.03, (d) 0.05, and (e) 0.08 wt%.

3.4. Effects of Rheological properties on vortex shedding

To consider the difference in the vortex shedding observed in the PEO solution and HPC solution, we compare the extensional rheological properties of these solutions and the period of vortex shedding. The extensional rheological property was represented by a relaxation time, λ [s], as measured under extensional stress with CaBER. The period of vortex shedding was calculated by a distance between two vortices that rotate in the same direction in the same side of the cylinder, L [m], and the mean velocity, V [m/s], as L/V [s]. The relaxation time of each solution and the period of vortex shedding of each flow are compared in Fig.7. The relaxation time of the PEO solution increased with the PEO concentration. The relaxation time is lower than the period of vortex shedding when the concentration of PEO is lower than 0.50×10^{-3} wt%. The relaxation time of 0.75×10^{-3} wt% PEO solution was almost the same as the period of vortex shedding. At this concentration, vortices almost disappeared when they were close to the comb. However, we observed weak vortices further downstream in test section 2. Therefore, it was possible to calculate the period of vortex shedding of Vortex-Type2. Near the concentration of 0.75×10^{-3} wt% of the PEO solution, the period of the vortex shedding was dominated by the relaxation time. This is considered as a lock-on phenomenon. The relaxation time exceeded the original period of vortex shedding when the concentration of PEO reached 1.0×10^{-3} wt%. In this regime, vortices were again shed from the cylinder. Nevertheless, the vortices that were shed in a solution at the high PEO concentration were different from the vortices observed in a solution at a low concentration. In the case of the HPC solution, the relaxation time of the solution is lower than the period of vortex shedding. Thus, the vortex shedding was not at all significantly affected by the HPC concentration. The relaxation time of each solution in the extensional flow clearly affects vortex shedding and deformation.

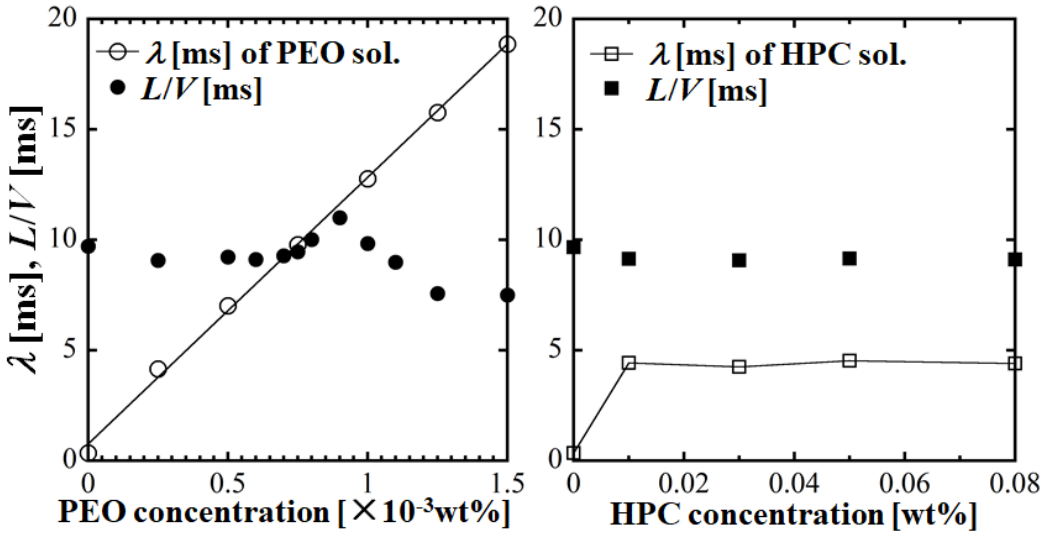

Fig.7 Relaxation time, λ [s], and period of vortex shedding, L/V [s].

3.5. Velocity fields and fluctuation intensity around the comb

To obtain additional information on vortex formation, we observed the velocity fields close to the comb with PIV measurements. Figure 8 shows the velocity fields of the polymer-free solution and PEO solution. High velocity fluctuation in the normal direction occurs close to the comb in the polymer-free solution. Conversely, PEO disturbed the local velocity fluctuation. The velocity fluctuation in the normal direction gradually diminished with the distance from the grid. In the 2D turbulent flow, vortices were shed at the comb, and subsequently the vortices were advected without significant deformation. Therefore, although the vortices were observed on the flow, the local velocity fluctuation approaches uniform velocity at the downstream.

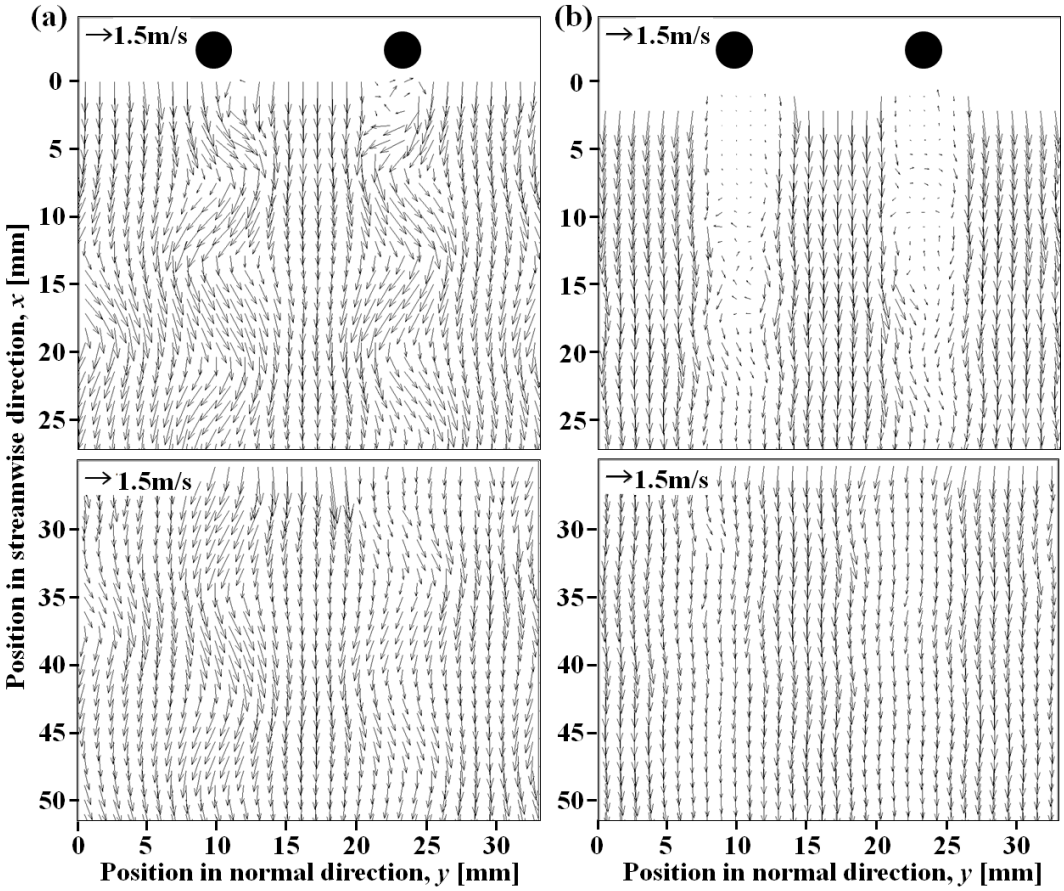

Fig.8 Velocity fields of (a) Polymer-free solution and (b) PEO 1.5×10^{-3} wt% solution

Figure 9 shows the vorticity fields of the polymer-free and PEO solutions, and these were calculated by the velocity fields. Positive and negative values of the vorticity alternatively shed at the comb, and swung when the concentration of PEO was low. The positive and the negative vorticities did not interact each other when the concentration of PEO was 0.75×10^{-3} wt%. The vorticity field was advected straight in the left and the right sides separately. The vorticity slightly enhanced again at the higher concentration of PEO at 1.5×10^{-3} wt% although vortices in the left and the right sides did not interact with each other. Thus, the vortices observed in PEO 1.5×10^{-3} wt% solution were different from those observed in the polymer-free and PEO 0.25×10^{-3} wt% solutions. The vorticity fields obtained from velocity fields are related to Vortex-Type1, Type2, and Type3 as visualized through the interference patterns of the flow. The relationship between the thickness of the 2D flow and the vorticity was suggested in a few previous studies [36, 39]. In this study, the thickness was determined using the interference patterns, and thus, the interference patterns are related to the vorticity. This was clearly observed in Figs.5, 6, and 9.

The vorticity fields shown in Fig. 9 also verify that the velocity field was not affected by the tracer particles.

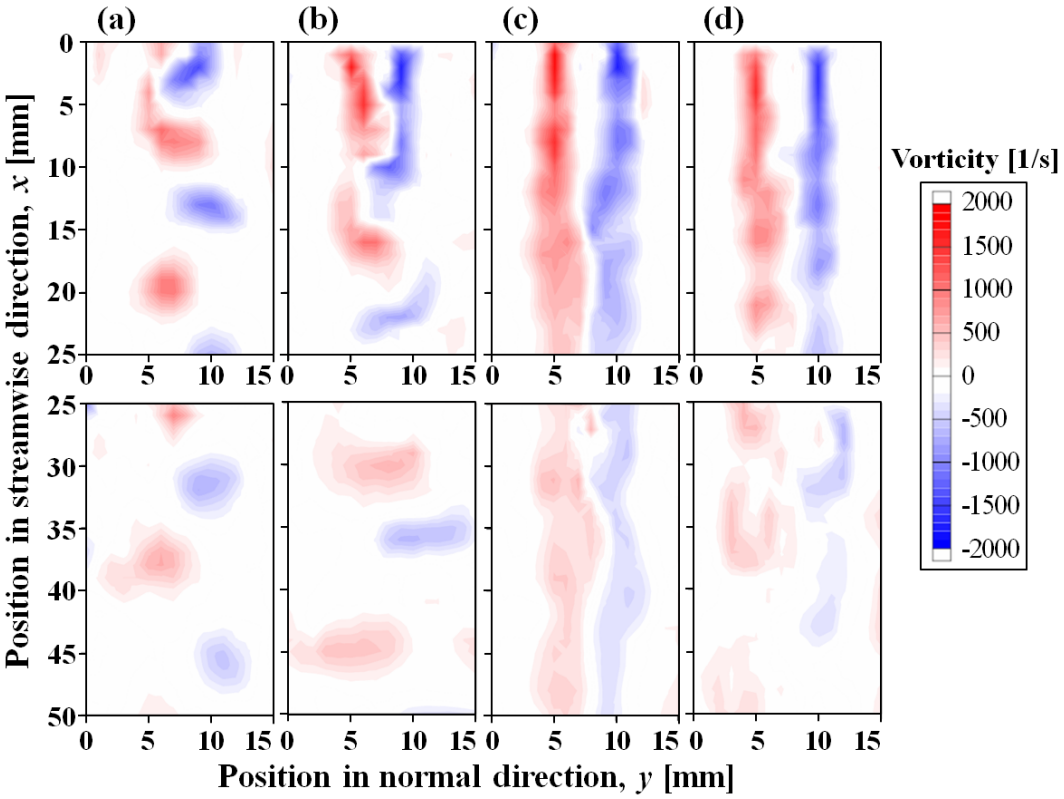

Fig.9 Vorticity fields of the polymer-free solution and PEO solution in test section 1. Given the recording limit of the high-speed camera, the data recording area close to the comb was separated into several parts. The figure shows examples of the areas from 0 mm to 25 mm and from 25 mm to 50 mm. Figure 9(a), 9(b), 9(c), and 9(d) show the respective vorticity fields of (a) polymer-free, (b) 0.25×10^{-3} wt%, (c) 0.75×10^{-3} wt%, and (d) 1.5×10^{-3} wt%, respectively.

To quantify the velocity fields, the fluctuation intensities in normal and streamwise directions were calculated using Eqs. (2) and (3). Figure. 10 shows the fluctuation intensity in the normal direction, FI_{V_y}, of the polymer-free solution and PEO solution at each downstream position. The horizontal axis denotes the normalized position in the normal direction: The position in the normal direction is normalized with the pitch of the cylinders. Thus, the origin in the horizontal axis in Fig. 10 corresponds to the centre of a cylinder: 1 in the axis corresponds to the centre of the neighbouring cylinder. There are two peaks in the figure: These peaks correspond to the normal positions behind the cylinder of the cylinders of the comb.

In the case of the polymer-free solution, the peak value of the fluctuation intensity was higher when the downstream position was closer. The peak value gradually decreased with the streamwise distance. When the concentration of PEO was 0.25×10^{-3} wt%, the average of the fluctuation intensity at each position was lower than that of the polymer-free solution, and the peak position shifted downstream. For example, the fluctuation intensity at 20 mm exceeded that at 10 mm with PEO 0.25×10^{-3} wt% solution. A similar tendency was observed when the concentration of PEO was lower than 0.75×10^{-3} wt%, and the average of the fluctuation intensity gradually decreased with increases in the concentration. When the concentration reached 0.75×10^{-3} wt%, the fluctuation of the flow was highly disturbed at all the positions due to the diminishing of the vortices. Vortex-Type3 was observed as shown in Figs. 5 (e) – 5 (g) when the concentration exceeded 0.75×10^{-3} wt%. However, Vortex-Type3 was different from Vortex-Type1 that was observed at a lower concentration of PEO. In the case of Vortex-Type3, two vortices aligned in two lines although the vortices disappeared in a short distance. This phenomenon was also confirmed with respect to the fluctuation intensity: Specifically, an original peak of a fluctuation intensity was split in two peaks as seen in the position at 10 mm and 20 mm downstream when the concentration of PEO was 1.5×10^{-3} wt% (Fig. 10(d)). However, these two peaks disappeared within a short distance. While the intensities at 10 mm and 20 mm exceeded those of 0.75×10^{-3} wt% (Fig. 10(c)) at the corresponding positions, the intensities further downstream were significantly lower and close to zero. Figure. 11 shows the streamwise variation in the maximum fluctuation intensities that correspond to the peak values observed at the respective normal distributions in Fig. 10. In the polymer-free case, the maximum streamwise position of the fluctuation intensity was extremely close to the cylinder, the peak value was extremely high, and the intensity decreased in the streamwise direction after the peak position. The streamwise variation in the intensity exhibited the same tendency as that in the polymer-free case when the concentration of PEO was lower than 0.50×10^{-3} wt%. However, the peak position shifted downstream, and the value decreased with the concentration. This peak shift corresponds to the wake expansion as shown in Fig. 5. In the case of 0.75×10^{-3} wt% of the PEO concentration, two weak peaks at 8 mm and 45 mm were observed in the figure although both values were extremely low and gradually decreased. When the concentration of PEO exceeded 1.0×10^{-3} wt%, a slightly higher peak appeared

near the cylinder, and the peak position also shifted downstream. The intensities in these cases exhibited a rather rapid decrease downstream and were low. These intensity behaviours correspond well to our observation as described above. As indicated in the results, the addition of PEO modified the vortex shedding and highly reduced the fluctuation in the vortices and the fluctuation intensity in the 2D flow.

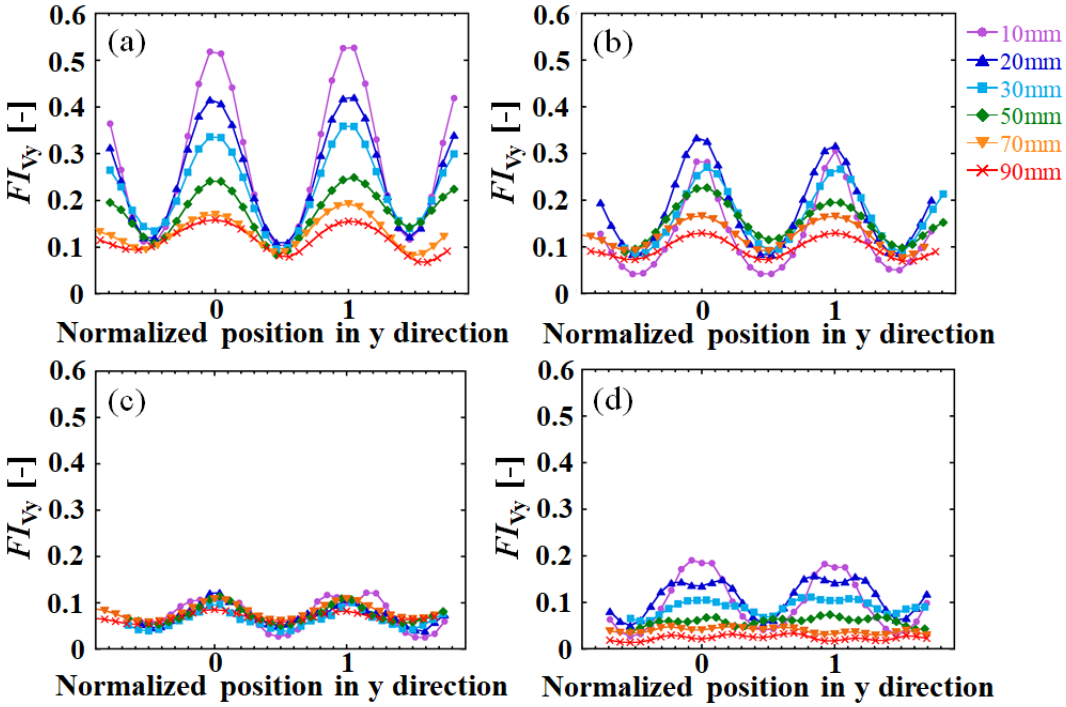

Fig.10 Fluctuation intensity in the normal direction of the polymer-free solution (a), and PEO solution at concentrations of (b) 0.25×10^{-3} wt%, (c) 0.75×10^{-3} wt%, and (d) 1.5×10^{-3} wt%.

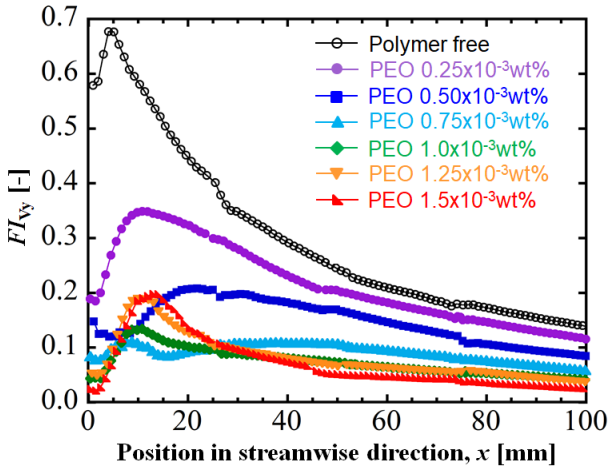

Fig.11 Maximum value of the fluctuation intensity in the normal direction of each PEO solution varied based on the distance from the comb.

The fluctuation intensities in the normal direction of the flow of the HPC solution are shown in Fig. 12. The fluctuation intensity slightly decreased with the HPC additives. The position where the vortices were generated moved downstream, and subsequently, the fluctuation intensity at 10 mm was lower than that at 20 mm in the case of 0.08 wt%. This phenomenon was similar to that of the PEO solution at lower concentrations. In the case of the HPC solution, vortices did not disappear even in the case of higher concentration of HPC in the present conditions.

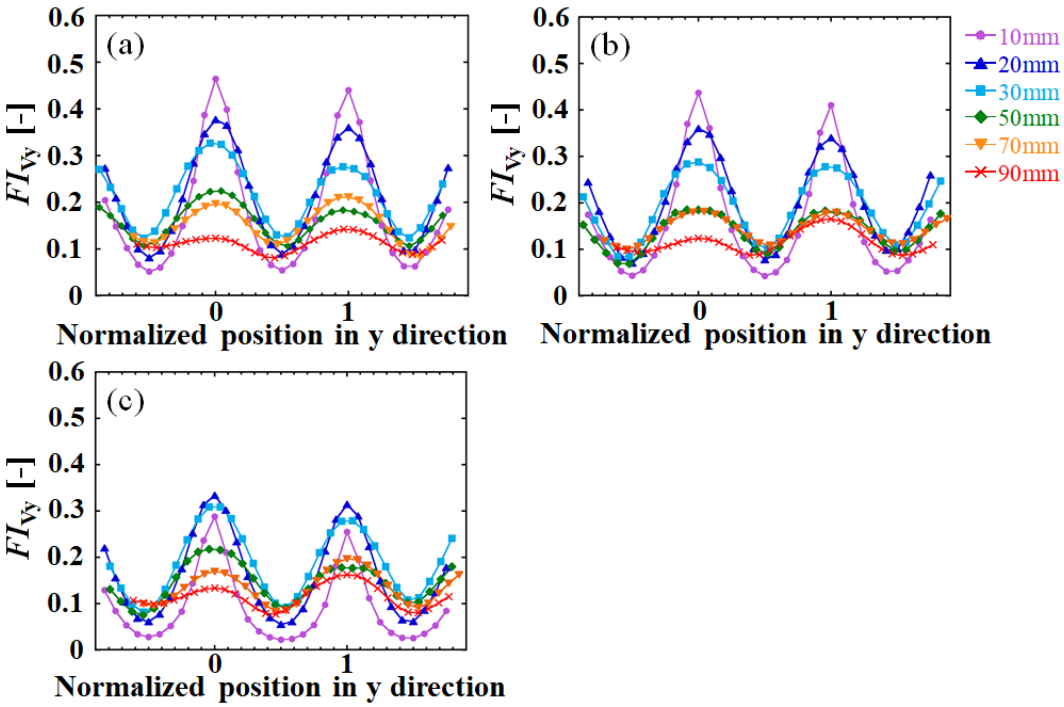

Fig.12 Fluctuation intensity in the normal direction of the polymer-free solution (a), and HPC solution at concentrations of (a) 0.03 wt%, (b) 0.05 wt%, and (c) 0.08 wt%.

The fluctuation intensities in streamwise direction, FI_{V_x}, are shown in Figs 13 and 14. Figure. 13 shows that of the PEO solution. The interesting point is that the maximum value of the intensity near the cylinder increased with the addition of PEO even in the case of 0.75×10^{-3} wt% when compared with those of the polymer-free case. The value of intensity gradually decreased with the distance although the fluctuation intensities at 20 mm and 30 mm of the PEO solution still exceeded those of the polymer-free solution at the corresponding positions. This is due to the wake expansion behind the cylinder and also the anisotropic effects of the polymers on the flow. Between the cylinders of the comb, the extensional deformation was

added to the fluid. This type of an extensional deformation causes flow instability in the streamwise direction based on the extensional properties of the fluid. As shown in Fig. 10, the normal fluctuation intensities were weakened by the PEO addition. These phenomena were observed in drag reducing flows. Therefore, the streamwise intensity was considered to increase the drag reducing flows due to the extensional effects of polymers and not due to the shear deformation of the fluids.

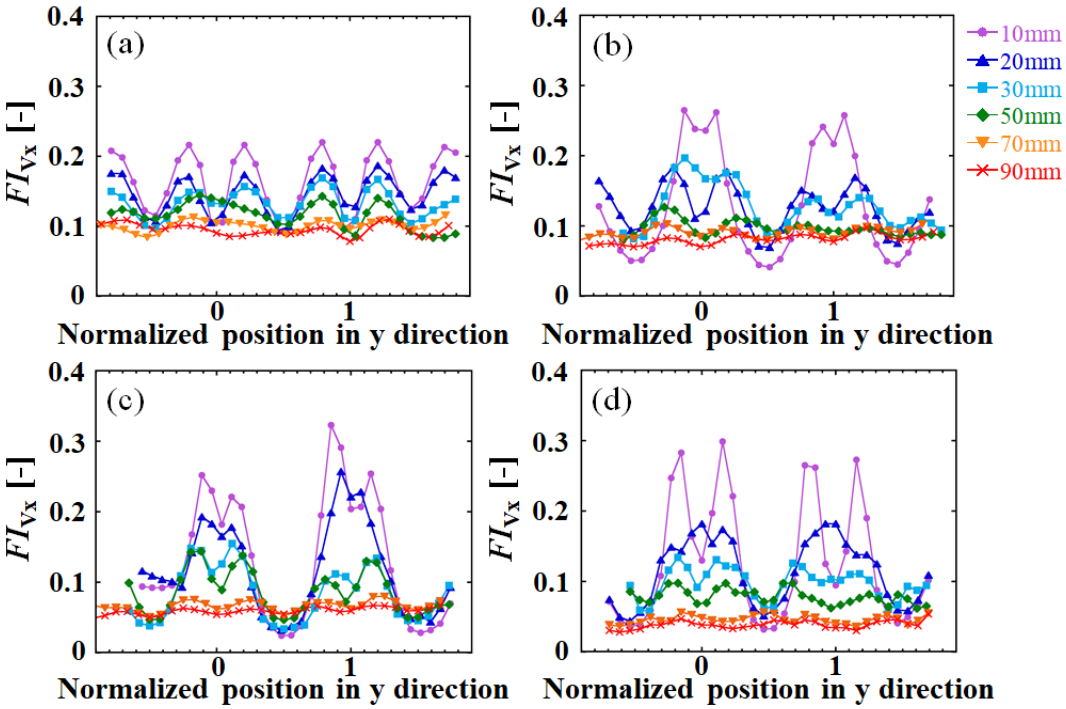

Fig.13 Fluctuation intensity in streamwise direction of the polymer-free solution (a) and PEO solution at concentrations of (b) 0.25×10^{-3} wt%, (c) 0.75×10^{-3} wt%, and (d) 1.5×10^{-3} wt%.

Figure 14 shows the fluctuation intensity in the streamwise direction of the HPC solution. The maximum value of the intensity increased at 10 mm from the comb, and this increased further with the HPC concentration. We consider this is simply due to the wake expansion behind the cylinder in which the mechanism is different from that of the PEO solution. This is because the intensity at 20 mm and beyond decreased when compared with that of the polymer-free solution.

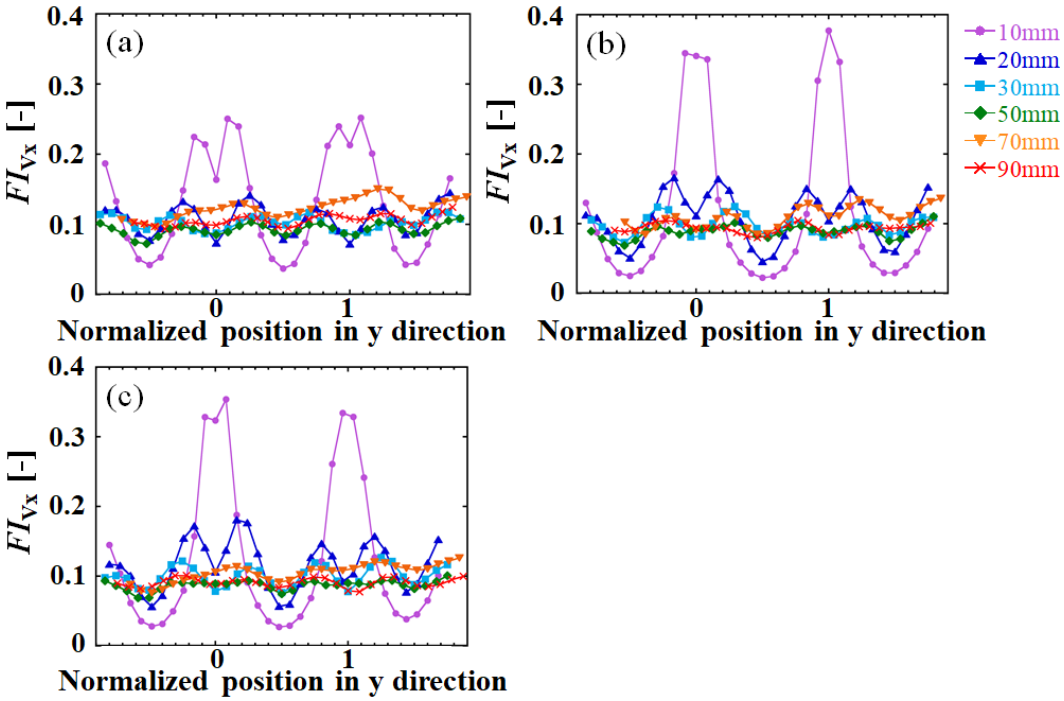

Fig.14 Fluctuation intensity in the streamwise direction of the HPC solution at the concentrations of (a) 0.03 wt%, (b) 0.05 wt%, and (c) 0.08 wt%.

We also calculated the Reynolds stress of each flow. Figure 15 shows the Reynolds stress of the polymer-free and PEO solution. In the case of the polymer-free solution, the maximum value was observed at 10 mm from the comb. The Reynolds stress was quickly diminished at distances corresponding to and exceeding 20 mm. In the case of the 0.25×10^{-3} wt% PEO solution, the Reynolds stress increased at 20 mm and 30 mm when compared with those of the polymer-free solution. This is due to wake expansion behind the cylinder. The Reynolds stresses of 0.75×10^{-3} wt% and of 1.5×10^{-3} wt% significantly decreased. The decrease in the Reynolds stress is typically observed in the drag reduction [3,6,22]. Figure 16 shows the Reynolds stress of the HPC solution. In the case of the HPC solution, the value increased at 10 mm and 20 mm. We attribute this to the wake expansion because the other tendency is the same as that of the polymer-free solution such as Vortex-Type1. The characteristics of the vortices were also detected by the Reynolds stress.

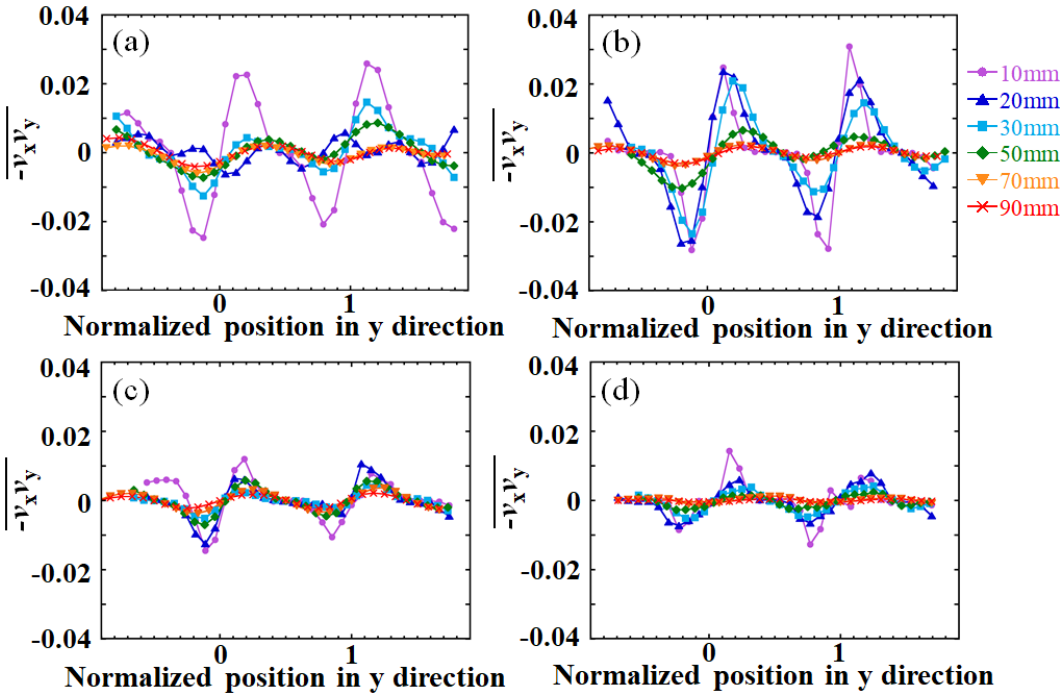

Fig.15 Reynolds stress of the polymer-free solution (a), and PEO solution at the concentrations of (b) 0.25×10^{-3} wt%, (c) 0.75×10^{-3} wt%, and (d) 1.5×10^{-3} wt%.

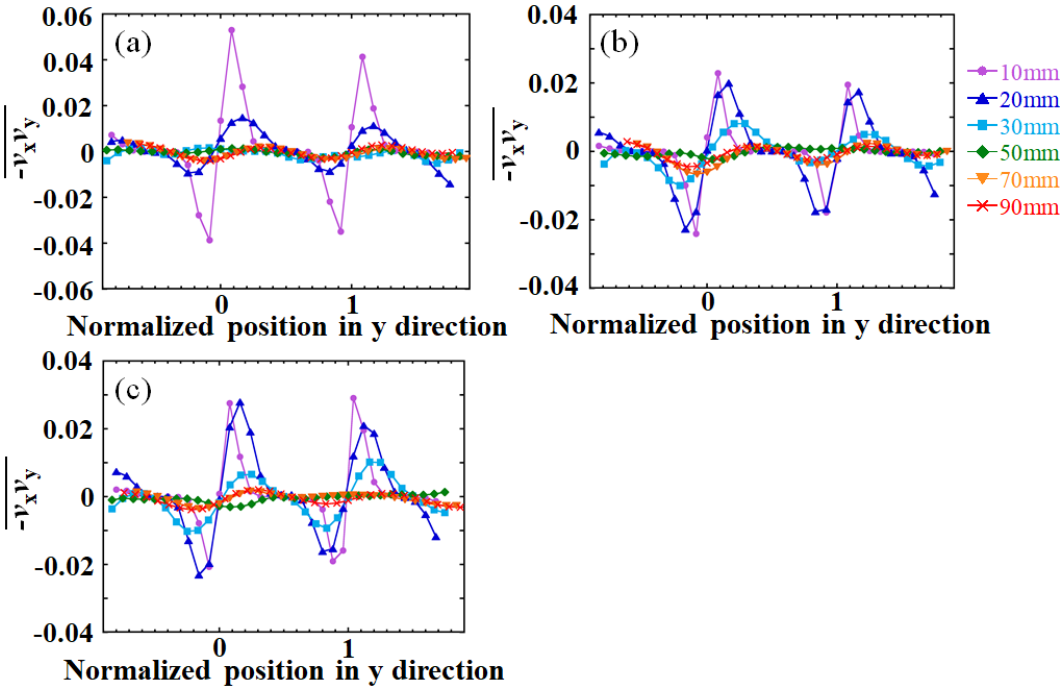

Fig.16 Fluctuation intensity in streamwise direction of the HPC solution at the concentrations of (a) 0.03 wt%, (b) 0.05 wt%, and (c) 0.08 wt%.

4. Conclusion

An experimental study was performed to investigate the relationship between the extensional rheological properties of polymer solutions and the 2D turbulent flow and vortex shedding on the 2D flow. The main conclusions of this study are as follows:

1. The scaling index of the power spectrum that is a passive scalar in 2D flow was calculated. The scaling index of the PEO solution significantly changed at a concentration of 0.75×10^{-3} wt% when the extensional rate was constant. Conversely, the scaling index of the HPC solution did not vary significantly. The effects of extensional rates on the scaling index of the PEO solution was also observed, and this was especially observed in the streamwise direction when the extensional rate increases. The results of the scaling index provided information on the energy transfer in 2D turbulent flow in the streamwise and normal directions.

2. The vortex shedding at the cylinder of the comb was visualized through interference patterns. The vortices shed at the cylinder were categorized into three types. When the PEO concentration was lower than 0.5×10^{-3} wt%, the wake region behind the cylinder expanded with increases in the polymer concentration, and the position where the vortex generation commenced shifted downstream. The vortices generated in this stage were categorized as Vortex-Type1. At the concentration of PEO 0.75×10^{-3} wt%, the vortex disappeared close to the cylinder. The vortex in the stage was categorized as Vortex-Type2. Vortex-Type3 appeared when the concentration of PEO exceeded 0.75×10^{-3} wt%: Vortex-Type3 was different from Vortex-Type1. Conversely, only Vortex-Type1 was observed in the case of the HPC solution.

3. The relaxation time affected vortex shedding, and this was quantified by a comparison of the period of vortex shedding, L/V [s], and relaxation time, λ [s]. The occurrence of Vortex-Type1, Type2, and Type3 were explained by the relationship between L/V [s] and λ [s]. Vortex-Type1 appeared when λ [s] was sufficiently lower than L/V [s]; Vortex-Type2 appeared when λ [s] was comparable to L/V [s]; Vortex-Type3 appeared when λ [s] exceeded L/V [s].

4. The difference between Vortex-Type3 and Type1 was also confirmed in terms of the fluctuation intensity and the Reynolds stress of the flow. Anisotropic phenomena of these vortices is due to polymer additives, and this was quantified.

We clarified the relationship between the extensional rheological properties of the polymer solution on vortex deformation on 2D turbulent flow. It is expected that this result will aid in further understanding drag reduction in terms of vortex deformation.

Acknowledgements

The present study was supported in part by a Grant-in-Aid for Young Scientists (A) (Project No.: 15H05552) from the Japan Society for the Promotion of Science (JSPS KAKENHI).

Reference

[1] P.S. Virk, E.W. Merrill, H.S. Mickley, K.A. Smith, E.L. Mollo-Christensen, The Toms phenomenon: turbulent pipe flow of dilute polymer solutions, J. Fluid Mech. 30 (1967) 305-328

[2] F.T. Pinho, J.H. Whitelaw, Flow of non-Newtonian fluids in a pipe, J. Non-Newtonian Fluid Mech. 34 (1990) 129-144.

[3] T. Wei, W.W. Willmarth, Modifying turbulent structure with drag-reducing polymer additives in turbulent channel flows, J. Fluid Mech. 245 (1992) 619-641.

[4] J.M. den Toonder, M.A Hulsen, G.D.C. Kuiken, F.T.M. Nieuwstadt, Drag reduction by polymer additives in a turbulent pipe flow: numerical and laboratory experiments, J. Fluid Mech. 337 (1997) 193-231.

[5] C. Wagner, Y. Amarouchene, P. Doyle, D. Bonn, Turbulent-drag reduction of polyelectrolyte solutions: Relation with the elongational viscosity, Europhys. Lett. 64 (2003) 823-829.

[6] M.P. Escudier, A.K. Nickson, R.J. Poole, Turbulent flow of viscoelastic shear-thinning liquids through a rectangular duct: Quantification of turbulence anisotropy, J. Non-Newtonian Fluid Mech. 160 (2009) 2-10.

[7] Z. Fu, T. Otsuki, M. Motozawa, T. Kurosawa, B. Yu, Y. Kawaguchi, Experimental investigation of polymer diffusion in the drag-reduced turbulent channel flow of inhomogeneous solution, Int. J. Heat and Mass Trans. 77 (2014) 860-873.

[8] M. Motozawa, T. Sawada, S. Ishitsuka, K. Iwamoto, H. Ando, T. Senda, Y. Kawaguchi, Experimental investigation on streamwise development of turbulent structure of drag-reducing channel flow with dosed polymer solution from channel wall, Int. J. Heat and Fluid Flow 50 (2014) 51-62.

[9] C.H. Hong, C.H. Jang, H.J. Choi, Turbulent drag reduction with polymers in rotating disk flow, Polymers 7 (2015) 1279-1298.

[10] P.S. Virk, Drag reduction by collapsed and extended polyelectrolytes, Nature 253 (1975) 109-110.

[11] P.S. Virk, D.C. Sherman, D.L. Wagger, Additive equivalence during turbulent drag reduction, AIChE J. 43 (1997) 3257-3259.

[12] S. Sasaki, Drag reduction effect of rod-like polymer solutions. I. Influences of polymer concentration and rigidity of skeletal back bone, J. Phys. Soc. Japan 60 (1991) 868-878.

[13] S. Sasaki, Drag reduction effect of rod-like polymer solutions. II. Comparison between microgel and linear type polyions, J. Phys. Soc. Japan 60 (1991) 2613-2618.

[14] S. Sasaki, Drag reduction effect of rod-like polymer solutions. III. Molecular weight dependence, J. Phys. Soc. Japan 61 (1992) 1960-1963.

[15] A. Japper-Jaafar, M.P. Escudier, R.J. Poole, Turbulent pipe flow of a drag-reducing rigid "rod-like" polymer solution, J. Non-Newtonian Fluid Mech. 161 (2009) 86-93.

[16] A.S. Pereira, R.M. Andrade, E.J. Soares, Drag reduction induced by flexible and rigid molecules in a turbulent flow into a rotating cylindrical double gap device: Comparison between Poly (ethylene oxide), Polyacrylamide, and Xanthan Gum, J. Non-Newtonian Fluid Mech. 202 (2013) 72-87.

[17] T. Min, J.Y. Yoo, H. Choi, D.D. Joseph, Drag reduction by polymer additives in a turbulent channel flow, J. Fluid Mech. 486 (2003) 213-238.

[18] Y. Dubief, C.M. White, V.E. Terrapon, E.S.G. Shaqfeh, P. Moin, S.K. Lele, On the coherent drag-reducing and turbulence-enhancing behaviour of polymers in wall flows, J. Fluid Mech. 514 (2004) 271-280.

[19] Y. Dubief, V.E. Terrapon, C.M. White, E.S.G. Shaqfeh, P. Moin, S.K. Lele, New answers on the interaction between polymers and vortices in turbulent flows, Flow, Turbulence and Combustion 74 (2005) 311-329.

[20] K.D. Housiadas, A.N. Beris, Extensional behavior influence on viscoelastic turbulent channel flow, J. Non-Newtonian Fluid Mech. 140 (2006) 41-56.

[21] M.D. Graham, Drag reduction and the dynamics of turbulence in simple and complex fluids, Phys. Fluids 26 (2014) 101301-1-24.

[22] S.-N. Wang, A. Shekar, M.D. Graham, Spatiotemporal dynamics of viscoelastic turbulence in transitional channel flow, J. Non-Newtonian Fluid Mech. 244 (2017) 104-122.

[23] A. Kushwaha, J.S. Park, M.D. Graham, Temporal and spatial intermittencies within channel flow turbulence near transition, Phys. Rev. Fluids 2 (2017) 024603-1-30.

[24] H. Kellay, X-L. Wu, W.I. Goldburg, Experiments with turbulent soap films, Phys. Rev. Lett. 74 (1995) 3975-3978.

[25] H. Kellay, W.I. Goldburg, Two-dimensional turbulence: a review of some recent experiments, Rep. Prog. Phys. 65 (2002) 845-894.

[26] G. Boffetta, R.E. Ecke, Two-dimensional turbulence, Annu. Rev. Fluid Mech. 44 (2012) 427-51.

[27] Y. Amarouchene, H. Kellay, Polymers in 2D turbulence: Suppression of large scale fluctuations, Phys. Rev. Lett. 89 (2002) 104502-104505.

[28] H. Kellay, Polymers suppress the inverse transfers of energy and the enstrophy flux fluctuations in two-dimensional turbulence, Phys. Rev. E. 70 (2004) 036310-036316.

[29] R. Hidema, H. Suzuki, S. Hisamatsu, Y. Komoda, H. Furukawa, Effects of the extensional rate on two-dimensional turbulence of semi-dilute polymer solution flows, Rheol. Acta 52 (2013) 949-961.

[30] R. Hidema, H. Suzuki, S. Hisamatsu, Y. Komoda, Characteristic scales of two-dimensional turbulence in polymer solutions, AIChE J. 60 (2014) 1854-1862.

[31] R. Hidema, H. Suzuki, I. Murao, S. Hisamatsu, Y. Komoda, Effects of extensional rates on anisotropic structures and characteristic scales of two-dimensional turbulence in polymer solutions, Flow Turbulence Combust. 96 (2016) 227-244.

[32] J.R. Cressman, Q. Bailey, W.I. Goldburg, Modification of a vortex street by a polymer additive, Phys. Fluids 13 (2001) 867-871.

[33] M.A. Rutgers, X-L. Wu, R. Bhagavatula, A.A. Petersen, W.I. Goldburg, Two-dimensional velocity profiles and laminar boundary layers in flowing soap films, Phys. Fluids 8 (1996) 2847-2854.

[34] R. Hidema, Z. Yatabe, M. Shoji, C. Hashimoto, R. Pansu, G. Sagarzazu, H. Ushiki, Image analysis of thickness in flowing soap films. I: effects of polymer, Exp. Fluids 49 (2010) 725-732.

[35] X.L. Wu, R. Levine, M. Rutgers, H. Kellay, W.I. Goldburg, Infrared technique for measuring thickness of a flowing soap film, Rev. Sci. Inst. 72 (2001) 2467-2471.

[36] M. Rivera, P. Vorobieff, R.E. Ecke, Turbulence in flowing soap films: Velocity, vorticity, and thickness fields, Phys. Rev. Lett. 81 (1998) 1417-1420.

[37] O. Greffier, Y. Amarouchene, H. Kellay, Thickness fluctuations in turbulent soap films, Phys. Rev. Lett. 88 (2002) 194101-194104.

[38] Y.L. Xiong, C.H. Bruneau, H. Kellay, A numerical study of two dimensional flows past a bluff body for dilute polymer solutions, J. Non-Newtonian Fluid Mech. 196 (2013) 8-26.

[39] P. Vorobieff, M. Rivera, R.E. Ecke, Soap film flows: Statistics of two-dimensional turbulence, Phys. Fluids 11 (1999) 2167-2177.